Nuclear quadrupole interaction in tin metal

G. S. Collins and N. Benczer-Koller
Department of Physics, Rutgers University, New Brunswick, New Jersey 08903
(Received 22 August 1977)

Precise Mössbauer measurements of the quadrupole splitting in tin metal over the range 4–450 K are reported. The analysis of the transmission spectra takes into account self-absorption effects in the emission profile and in the absorption, as well as line-broadening due to source granularity. At 296 K, $e^2Qq/h = -9.73(40)$ MHz, in good agreement with a time-differential-perturbed-angular-correlation measurement. The splitting decreases by 25% over the temperature range studied. The experimental electric-field gradient is compared with calculations of the lattice and conduction-electron contributions. Results from augmented-plane-wave calculations of the electronic contribution in which the effects of lattice vibrations were explicitly considered are briefly reported, and the axial ratio dependences of the two contributions are discussed.

I. INTRODUCTION

The mechanisms producing the electric-field gradient (EFG) at the nucleus in the noncubic metals have been the subject of considerable experimental and theoretical work recently. The interaction frequency e^2Qq/h of the nuclear quadrupole moment Q with the electric-field gradient eq and its temperature dependence may be measured by a variety of techniques, such as the Mössbauer effect, time differential perturbed angular correlation (TDPAC), or nuclear resonance, but neither Q nor eq can as yet be reliably calculated from first principles to an accuracy better than about 30%. When Q is known for the nuclear level of interest, the EFG at the nucleus may be derived from the observed interaction frequency e^2Qq/h.

In the axial noncubic metals two terms contribute to the EFG,

$$eq = eq_{\text{latt}}(1-\gamma_\infty) + eq_{\text{ce}}(1-R) \quad , \tag{1}$$

where eq_{latt} is the gradient caused by the lattice of metal ions, shielded by the Sternheimer factor γ_∞ of the probe ion core, and eq_{ce} is caused by the conduction electrons. Published values of γ_∞ for free closed-shell ions[2] are generally used for ions embedded in solids. These factors are quite large for heavy ions. The shielding factor R for the valence electrons is usually small,[3] $|R| \sim 0.1$, and is neglected below. The contribution eq_{latt} may be calculated by well-known lattice-sum methods.[4] Empirically, eq_{ce} has been observed to be about three times larger than $eq_{\text{latt}}(1-\gamma_\infty)$ and of opposite sign.[5]

Calculations of eq_{ce} have been made by band-structure methods for nontransition sp-band metals.[1,6] In these metals, eq_{ce} arises from the electron density of perturbed-plane-wave conduction-electron states. In noncubic transition metals and at transition-metal probes, the d states cause strong perturbations in the free-electron states which are less amenable to calculation.

Interaction frequencies e^2Qq/h have been measured at many impurity probes embedded in the noncubic metals as well as at host-metal atoms themselves. Experimental results from the latter measurements may be more appropriate for theoretical analysis since the electron density near a host-probe nucleus is unperturbed by local size or valency effects which may be expected near an impurity-probe ion.

In the present experiment, e^2Qq/h was measured in tin metal as a function of temperature using the Mössbauer level of ^{119}Sn, for which the quadrupole moment $Q = -0.06(2)$ b is known.[7] Tin, which has the D_{4h}^{19} structure, is one of the few noncubic sp-band metals which is not hexagonal close packed. It is of particular interest since, as will be shown below, $eq_{\text{latt}}(1-\gamma_\infty)$ is only about $(\frac{1}{20})$th of the measured EFG, in contrast to the empirical ratio $\frac{1}{2}$ which has been observed in many hcp metals.[5] Also, while the total gradient decreases by about 25% over the range 4–500 K, the lattice gradient increases by more than a factor of 2, and the ratio eq/eq_{latt} varies by a factor of 3.

Earlier Mössbauer measurements at ^{119}Sn in tin[8] are in poor agreement with each other and the temperature dependence of e^2Qq/h has not been well established. The Mössbauer measurements are difficult to analyze since the quadrupole splitting is only about one-half of the spectral linewidth (Fig. 1). In particular, careful analysis of the transmission line shape is required, including treatment of the effects on the line shape caused by resonant self-absorption in the source and absorber, and granularity of the source material. These effects, which tend to broaden the absorption spectrum, were considered in detail in the present investigation.

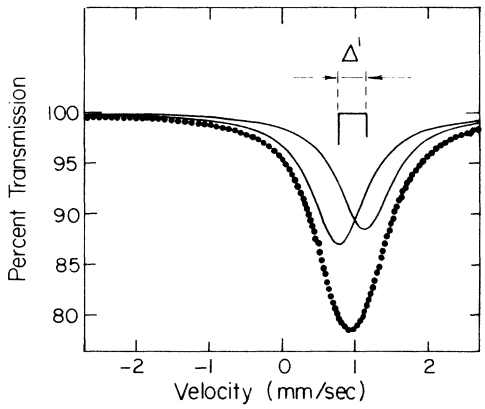

FIG. 1. Typical ^{119}Sn Mössbauer spectrum obtained with a V-Sn source and a 24-μm-thick tin absorber at 118 K. The curves were obtained from a computer fit to a sum of two Lorentzian lines.

Experimental details are described in Sec. II and relevant parts of the theory of the Mössbauer line shape are reviewed in Sec. III. Effects of source granularity are also presented in Sec. III using simple models described in Appendix A. The quadrupole splittings were obtained by fitting both experimental and theoretical spectra to sums of two Lorentzians and comparing graphically the spectral parameters obtained in each case; the results are presented in Sec. IV. The experimental EFG is compared with calculations of the lattice and conduction-electron contributions in the final section. The contribution eq_{ce} was calculated by the augmented-plane-wave method. The axial ratio dependences of eq_{latt} and eq_{ce} in tin metal are also discussed.

II. EXPERIMENT

Mössbauer spectra were measured in transmission geometry using a constant-acceleration spectrometer of standard design. The 23.871-keV Mössbauer γ rays were detected in a 0.1-cm-thick NaI(Tl) scintillation detector with a 50-μm-thick Pd critical absorber located halfway between source and detector. The source-detector solid angle was less than 0.02 sr in all measurements. Spectra were accumulated in a 400-channel multichannel analyzer running in time mode and synchronized to the triangular waveform of the source transducer. In the computer analysis of each run, the mirror-image spectra of 200 channels were fitted separately and the two sets of fitted parameters were subsequently averaged. About 10^6 counts per channel were accumulated during each run to ensure good statistics.

Three different ^{119}Sn^m Mössbauer sources were employed during the experiment.[9] Two consisted of $BaSnO_3$ powder prepared with neutron-activated ^{118}Sn and encapsulated in lucite; the third was a dilute alloy of tin in vanadium prepared by electroplating the ^{119}Sn^m activity onto a 0.025-cm-thick vanadium foil and diffusing the tin into the foil. The activity in the V-Sn alloy source was uniformly distributed, as evidenced by equal γ-ray emission rates from both sides of the foil. Source activities were measured with a scintillation detector, taking into account the mass absorption of the air between source and detector and the self-absorption in the sources. The ratio of the recoilless fractions for emission f, of the V-Sn and the $BaSnO_3$ sources was found to be 0.67(1) at room temperature by comparing spectral areas from the Mössbauer measurements made with identical absorbers. Using the value[10] $f_s(BaSnO_3)=0.65$, the value $f_s(V\text{-}Sn)=0.44$ is found. The relevant parameters characterizing the three sources are listed in Table I.

The tin metal absorbers were combinations of rolled polycrystalline foils[11] with thicknesses of 5 μm ($m3N$), 24 μm, and 130 μm ($m5N$) which were determined by weighing foils of measured areas. The absorbers were mounted either in a liquid-helium cryostat or in a cryostat-oven with thermal connection to a cold finger and an electrical heater. Temperatures were monitored with thermocouples and a Ge resistance thermometer and were constant to within ± 2 K during each run. The sources were kept at room temperature.

III. MÖSSBAUER LINE SHAPE

The general theory of the transmission Mössbauer line shape was originally given in Ref. 12 and is applied here for the case in which the emission profile is unsplit and the absorption cross section has a quadrupole splitting $E_Q=\frac{1}{2}e^2Qq$. Relevant parameters for ^{119}Sn are the transition energy[13] $E_0=23.871(7)$ keV, the mean life of the Mössbauer level[14] $\tau=25.87(10)$ nsec, and the maximum resonant γ-ray absorption cross section per nucleus[13] $\sigma_0=1.403(23)\times10^{-18}$ cm^2 at the transition energy. The natural width

$$\Gamma_0=\hbar/\tau=2.544(10)\times10^{-8}eV$$

is equal to 0.3195(12) mm sec^{-1} in velocity units and 6.151(24) MHz in frequency units.

A. Doublet line shape

For a source moving at velocity v toward a stationary absorber, the transmission line shape is given by

$$\epsilon(v)=[N_\infty-N(v)]/N_\infty\ , \tag{2}$$

where $N(v)$ and N_∞ are the counting rates at velocity v and at a velocity far off resonance. If E is the γ-ray energy, and $W_v(E)$ the recoilless emission profile

TABLE I. Mössbauer source parameters.

Source matrix	*A* $BaSnO_3$	*B* $BaSnO_3$	*C* V-Sn
Source activity (mCi)	4.8	5.0	7.0
Specific activity (mCi/g)	190	314	484
^{119}Sn isotopic abundance	1.9%	0.76%	0.75%
Source area (cm^2)	1.13	1.13	2.01
Recoilless fraction: f_s	0.65[a]	0.65[a]	0.44[b]
Average source thickness[c] (μm)	79	51	250
	Average absorption thickness parameters		
Resonant thickness:[d] t_s	1.95	0.50	0.17
Nonresonant thickness:[e] t_s^{nr}	0.77	0.49	1.64
Thickness ratio $m = t_s^{nr}/t_s$	0.39	0.98	9.8
	Spectral linewidths $\Gamma(0)/\Gamma_0$ extrapolated to $t_a = 0$		
Calculated[f] $\Gamma(0)_{calc}/\Gamma_0$	2.465	2.120	2.031
Experimental[g] $\Gamma(0)_{expt}/\Gamma_0$	2.63(1)	2.26(1)	2.12(11)
Difference $[\Gamma(0)_{expt} - \Gamma(0)_{calc}]/\Gamma_0$	0.165	0.14	0.09

[a]Reference 10.

[b]From the ratio $f_s(\text{V-Sn})/f_s(BaSnO_3) = 0.67(1)$, obtained in this experiment.

[c]Obtained with $\rho(BaSnO_3) = 7.2$ g/cm^3 and $\rho(\text{V}) = 6.0$ g/cm^3.

[d]Resonant thickness parameters for ^{119}Sn may be calculated using $t = 7.12 d f_s$ in which d is the area density of ^{119}Sn in mg/cm^2 in the source or absorber.

[e]Mass-absorption cross sections of the elements Ba, Sn, O, and V at 23.8 keV used were obtained from *Handbood of Chemistry and Physics*, 53rd ed., edited by R. O. Weast (Chemical Rubber Co., Cleveland, 1972), p. E-126.

[f]Values quoted were calculated numerically from t_s and m by solving $W_c(x) = \frac{1}{2} W_c(0)$ for $x = \Gamma_s/\Gamma_0$.

[g]See Sec. IV.

from the source, the transmission can be written in terms of the dimensionless variables[15] $x = 2(E - E_0)/\Gamma_0$ and $y = 2vE_0/c\Gamma_0$ as the convolution integral

$$\epsilon(y) = \text{const} \int W_c(x+y)\{1 - \exp[-t_a A(x)]\}\, dx \quad , \tag{3}$$

where $A(x)$ is the resonant absorption cross section; $t_a = n_a \sigma_0 f_a$ is the dimensionless resonant absorption thickness parameter, with n_a the number of ground-state Mössbauer nuclei per unit area in the absorber; and f_a the average recoilless fraction in the absorber.

In the absence of splitting, $A(x)$ is equal to the Lorentzian function

$$l(x) = 1/(1+x^2) \quad . \tag{4}$$

In the axially symmetric electric-field gradient found in tin metal, the excited state is split and $A(x)$ is given by

$$A(x) = b_{3/2} l(x - E_Q/\Gamma_0) + b_{1/2} l(x + E_Q/\Gamma_0) \quad . \tag{5}$$

The coefficients b indicate the relative probabilities of excitation to the $\pm\frac{3}{2}$ and $\pm\frac{1}{2}$ substates of the Mössbauer level[16] ($b_{3/2} + b_{1/2} = 1$) and are determined by the multipolarity of the radiation field ($M1$ for ^{119}Sn), the vibrational anisotropy (Goldanskii-Karyagin effect), and texture effects arising from preferred orientation of the crystallite axes in a polycrystalline absorber.[17]

For an $M1$ transition with angle θ between the principal axis of the EFG at the absorber nucleus and the direction of the incident γ ray, the ratio of the probabilities b is

$$\frac{b_{3/2}}{b_{1/2}} = \frac{1 + \frac{1}{2}P_2(\cos\theta)}{1 - \frac{1}{2}P_2(\cos\theta)} \quad . \tag{6}$$

In an axial crystal the mean-square displacement $\langle x^2 \rangle$ of an atom depends on the angle θ, and expressed in terms of its components along and perpendicular to the EFG axis is

$$\langle x^2 \rangle = \langle x_\perp^2 \rangle + (\langle x_\parallel^2 \rangle - \langle x_\perp^2 \rangle)\cos^2\theta \quad . \tag{7}$$

The recoilless fraction f_a as a function of angle is then given by

$$f_a(\theta) = \exp(-k^2\langle x^2\rangle) \ , \tag{8}$$

where k is the wave number of the γ ray. Over a random distribution of angles θ in a polycrystalline absorber, the average value of $f_a(\theta)$ is

$$f_a = \tfrac{1}{3}[f_a(0) + 2f_a(\tfrac{1}{2}\pi)] \ . \tag{9}$$

In general, the expectation value R_Q of the intensity ratio of the two absorption lines is given by

$$R_Q = \frac{\langle b_{3/2}\rangle}{\langle b_{1/2}\rangle} = \int_0^\pi [1 + \tfrac{1}{2}P_2(\cos\theta)] f_a(\theta) D(\theta) \sin\theta \, d\theta \times \left(\int_0^\pi [1 - \tfrac{1}{2}P_2(\cos\theta)] f_a(\theta) D(\theta) \sin\theta \, d\theta \right)^{-1} , \tag{10}$$

where $D(\theta)$ is the distribution of crystallite axes in the absorber. Finally, the resonant absorption cross section may be written

$$A(x) = \frac{R_Q}{1+R_Q} l\left(x - \frac{E_Q}{\Gamma_0}\right) + \frac{1}{1+R_Q} l\left(x + \frac{E_Q}{\Gamma_0}\right) . \tag{11}$$

B. Emission profile

In the $BaSnO_3$ and V-Sn sources the symmetry at the tin site is cubic so that there is no quadrupole splitting in the sources, and the γ rays are emitted by the ensemble of excited state nuclei with probability $(1/\pi) l(x)$. The recoilless distribution emitted from a uniform source is found upon integrating over source thickness[12] the product of the probability for emission by the probability for self-absorption of γ rays in the source

$$W_e(x) = \frac{f_s}{\pi t_s} \int_0^1 l(x) \exp\{-t[t_s^{nr} + t_s l(x)]\} \, dt \ , \tag{12}$$

in which t is a dimensionless variable of integration with limits 0 and 1 corresponding to the back and front surfaces of the source. The resonant absorption thickness parameter for the source t_s is given by $t_s = n_s \sigma_0 f_s$, where n_s is the number of ground-state Mössbauer nuclei per unit area in the source, and f_s is the recoilless fraction in the source. The nonresonant absorption thickness parameter

$$t_s^{nr} = \sum_i \mu_i n_i$$

is the sum of products for each element in the source (Ba, Sn, O, and V) of the nonresonant absorption cross section μ_i per atom at 23.871 keV of each element by the number n_i of atoms per unit area. The ratio $m = t_s^{nr}/t_s$ is a convenient parameter which is used subsequently, and which depends only on the composition of the source.

Equation (12) can be integrated directly to obtain

$$W_e(x; t_s, m) = \frac{f_s}{\pi t_s} \frac{l(x)}{m + l(x)} \times (1 - \exp\{-t_s[m + l(x)]\}) \tag{13}$$

in terms of the thickness ratio m. In the limits of small and large t_s, $W_e(x)$ has a Lorentzian shape with full width at half-maximum Γ_s given by Γ_0 and $\Gamma_0(1 + 1/m)^{1/2}$, respectively. For intermediate t_s, the line shape remains approximately Lorentzian and the width may be found by solving the equation $W_e(x) = \frac{1}{2} W_3(0)$ numerically. Figure 2 shows the variation of Γ_s with t_s for selected values of m; for any given $m \neq 0$ and with increasing t_s, the width approaches the limiting value $\Gamma_0(1 + 1/m)^{1/2}$, due to the attenuation of γ rays emitted from deep within the source by the nonresonant absorption. For $m = 0$, Γ_s is described by the linear relation $\Gamma_s = \Gamma_0(1 + 0.295 t_s)$ to an accuracy of 2% over the range $t_s = 0$–4. As there is often substantial nonresonant self-absorption in Mössbauer sources, this linear relation obtained for $m = 0$ is not generally valid.

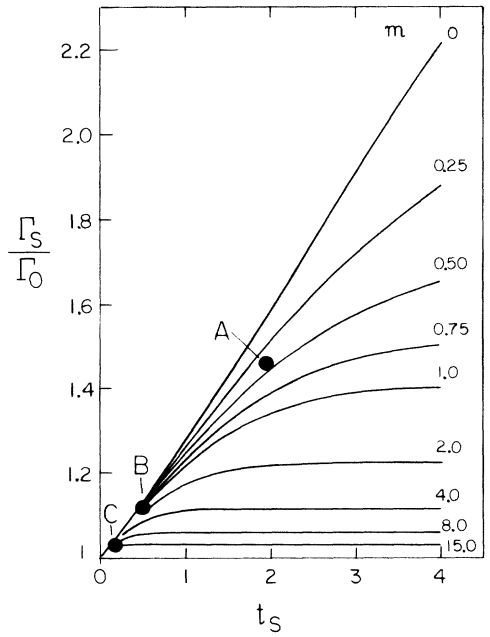

FIG. 2. Dependence of the emission linewidth from a uniform Mössbauer source on the source resonant absorption thickness t_s for values of the parameter $m = t_s^{nr}/t_s$ where t_s^{nr} is the nonresonant absorption thickness. The data points show the line broadening of the three sources used in the experiment.

The data points in Fig. 2 show the linewidths for the three sources derived from the average source thickness parameters t_s and m (Table I). In the limit of zero-absorber thickness, the linewidth $\Gamma(0)$ of each component line of the transmission spectrum should be equal to $\Gamma_s + \Gamma_0$, as the factor $\{1 - \exp[-t_a A(x)]\}$ in Eq. (3) is equal to $t_a A(x)$, and the integral becomes equal to the sum of two convolution integrals of Lorentzian of widths Γ_s and Γ_0. The values for $\Gamma(0)$ computed using the average source parameters (Table I) of sources A, B, and C by solving for $x = \Gamma_s/\Gamma_0$ in the equation $W_e(x;t_s,m) = \frac{1}{2} W_e(0;t_s,m)$ were $2.465\Gamma_0$, $2.120\Gamma_0$, and $2.031\Gamma_0$, respectively. The experimental values for $\Gamma(0)$ determined for the sources (see Fig. 3 and Sec. IV) were $2.63(1)\Gamma_0$, $2.26(1)\Gamma_0$, and $2.12(1)\Gamma_0$, respectively. The discrepancy between the calculated and experimental values of $\Gamma(0)$ is considerably larger for the two stannate sources than for the V source. For source C, which was quite uniform in composition and in thickness, the difference $\Gamma(0)_{\text{expt}} - \Gamma(0)_{\text{calc}} = 0.09\Gamma_0$. This small broadening, about 5% of the spectral linewidth, could not be explained and might be of instrumental origin. It was assumed that for the stannate sources the same broadening also occurred. By subtracting $0.09\Gamma_0$ from the experimental linewidths $\Gamma(0)$, the values of $\Gamma_s + \Gamma_0$ were obtained, yielding Γ_s equal to $1.54\Gamma_0$, $1.17\Gamma_0$, and $1.03\Gamma_0$ for sources A, B, and C, respectively. These corrected experimental values for Γ_s represent entirely the line-broadening mechanisms in the sources.

Most of the additional broadening in the stannate sources may be attributed to the granularity of the source material. The $BaSnO_3$ sources A and B were examined under a microscope and found to be composed of grains with distributions of sizes varying from 0.1 to 2.5 times the average thicknesses of the sources. The effects of this granularity on the emission profile, and particularly on the emission linewidth, have been estimated in Appendix A using simple models. It was found that when the ratio r of the mean thickness of a grain to the average thickness of the source (assumed uniform) is greater than about unity, the emission profile is well described by Eq. (13) using an effective thickness parameter t_s^{eff} which is larger than t_s, resulting in a correspondingly larger line broadening. The observed linewidths of the stannate sources are shown in Appendix A to be consistent with average grain sizes equal to about 1.2 times the average source thicknesses, in agreement with the rough visual observations. Thus, only 5% of the spectral linewidths observed could not be accounted for by this line shape theory. Effects of resonant self-absorption in the absorbers on the experimental line shape are considered in Sec. IV.

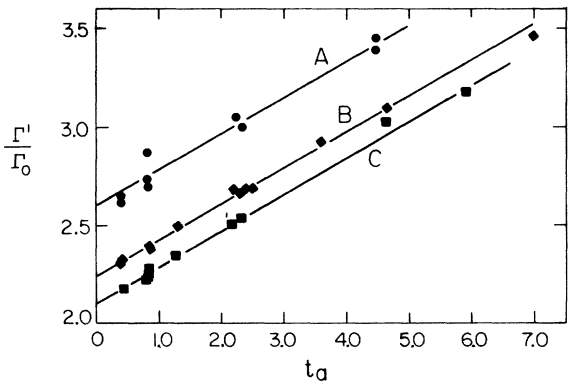

FIG. 3. Variation of the fitted linewidths of the doublet Lorentzian lines with the resonance thickness parameter t_a obtained with sources A, B, and C and tin metal absorbers at 296 K.

IV. DATA ANALYSIS

The quadrupole splitting $\frac{1}{2}e^2Qq$ was obtained from analysis of the experimental spectra by a graphical method. Similar techniques have been used in other Mössbauer studies.[18]

The experimental spectra were fitted by computer to a sum of two Lorentzians

$$\epsilon(y) = \frac{R'}{1+R'} I\left[\left(y - \frac{\Delta'}{\Gamma_0}\right)\left(\frac{\Gamma_0}{\Gamma'}\right)\right] + \frac{1}{1+R'} I\left[\left(y + \frac{\Delta'}{\Gamma_0}\right)\left(\frac{\Gamma_0}{\Gamma'}\right)\right], \tag{14}$$

in which the splitting Δ', the linewidth Γ' of the two lines, and the intensity ratio R' of the two lines were freely varied parameters. $I(x)$ was defined by Eq. (4). In addition, the counting rate off resonance, the magnitude of the absorption dip, and the centroid of the spectrum were fitted.

When, as for the case of tin metal, the absorption function $A(x)$ is the sum of two largely overlapping Lorentzians (Fig. 1), the splitting Δ' obtained from a fit to a sum of Lorentzians overestimates the true hyperfine splitting because of effects of saturation in the resonant abosrption. The true quadrupole splitting E_Q was deduced from Δ' in the following manner. Theoretical spectra were computed by numerical integrations of Eq. (3) over large ranges of physical parameters E_Q, R_Q, t_a, t_s, and m. Integrations were carried out over 198 evenly spaced energies by repeated application of the Newton-Cotes six-point closed-interval formula. The computed spectra were fitted just like the experimental spectra, to a sum of two Lorentzians, to obtain the theoretical parameters Δ, Γ, and R.

Graphs were prepared showing the relations between Δ, Γ, and R and the physical parameters. The parameters Δ', Γ', and R' obtained from the computer fits of the experimental spectra were plotted on the same graphs, and the corresponding real physical values of the various parameters were obtained by graphical interpolation.

Some approximate relations exist between Δ, Γ, and R and the source parameters t_s and m which simplify the analysis. The splitting Δ depends almost entirely on absorber thickness and on E_Q: in general, Δ is equal within 2% to the value obtained for $t_s=0$ as long as $t_s < 3E_Q/\Gamma_0$. The splitting is also independent of R_Q. Furthermore, to a good approximation the linewidth may be written as the sum of two terms $\Gamma=\Gamma_s+\Gamma_a$, in which Γ_s is the emission linewidth (Sec. III), and Γ_a is the width contributed by resonant self-absorption in the absorber. The width Γ_a depends only on t_a and E_Q. Finally, the intensity ratio R depends in a more complicated way on the three absorber parameters but is independent of source parameters. These relationships are summarized in the following expressions: $\Delta=\Delta(E_Q,t_a)$,

$$\Gamma=\Gamma_s(t_s,m)+\Gamma_a(t_a,E_Q) \ ,$$

and $R=R(R_Q,t_a,E_Q)$. Since only Γ is influenced significantly by source parameters, the graphs prepared for $t_s=0$ may be used for the analysis if the experimental linewidths Γ' are first corrected for emission and instrumental line broadening before comparison with the graphs.

The parameters Γ_s were obtained experimentally for each source from the widths Γ' measured at room temperature on different absorber thicknesses of tin metal. The data and linear fits are shown in Fig. 3 for the three sources and the extrapolated linewidths $\Gamma(0)$ obtained are given in Table I. The resonant absorption parameter t_a was calculated for each absorber with[19] $f_a=0.04$. The source and instrumental line broadening is empirically equal to $\Gamma(0)_{\text{expt}}-2\Gamma_0$, and the fitted widths Γ' were corrected for source broadening by subtracting those difference.

In Fig. 4 the dependences of Δ and Γ on E_Q and t_a are displayed over a wide range. Also shown are the data obtained from the series of measurements at room temperature with source B and with tin metal foil absorbers of thicknesses 24, 48, 72, 130, 202, 261, and 391 μm. The observed splittings are consistent with a single value $E_Q \sim 0.83(2)\Gamma_0$. From the variation of t_a with absorber thickness, $f_a=0.040(2)$ was deduced, which agrees well with[19,20] $f_a=0.040$ at 296 K. This agreement, as well as the consistency in E_Q for splittings Δ that vary by more than 50%, supports this graphical method of analysis. It is to be noted that both E_Q and t_a may in principle be found directly from the linewidth Γ and splitting Δ using Fig. 4, but caution must be exercised when the absorber exhibits a significant amount of granularity.[21]

Figures 5 and 6 show separately the variations of Δ and Γ on t_a for various values of E_Q. The data are the same as for Fig. 4, with t_a calculated using $f_a=0.04$. From Fig. 5 $E_Q/\Gamma_0=0.828(23)$ was found; with less precision, Fig. 6 indicated $E_Q/\Gamma_0=0.75(20)$. The data in these figures further support the value

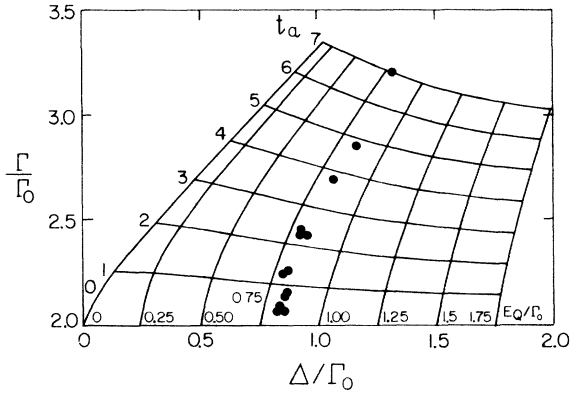

FIG. 4. Graph showing the dependences of the spectral splitting Δ and linewidth Γ obtained from computer fits of calculated spectra to sums of two Lorentzian lines on the absorber thickness t_a and the quadrupole splitting E_Q. The graph was computed for $t_s=0$. The data are results from room-temperature measurements with source B and tin metal absorbers of different thicknesses. The linewidths shown have been corrected for broadening of the emission line.

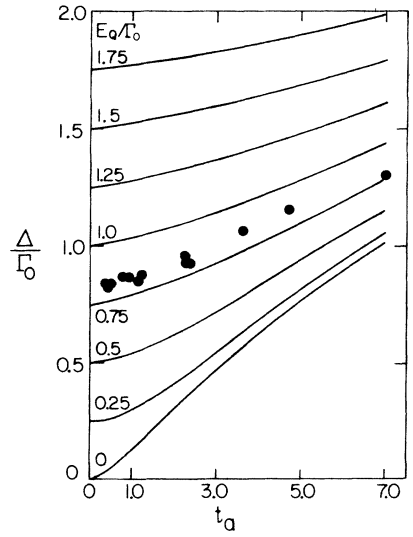

FIG. 5. Dependence of the fitted splitting on absorber thickness and the quadrupole splitting E_Q. The curves were prepared from fits to calculated spectra (see text). Data are the same as in Fig. 4 (see caption) with $f_a=0.040$ used to calculate t_a.

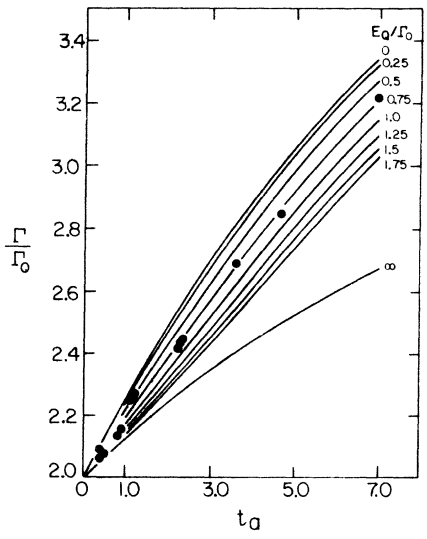

FIG. 6. Dependence of the fitted linewidth on absorber thickness and the quadrupole splitting E_Q.

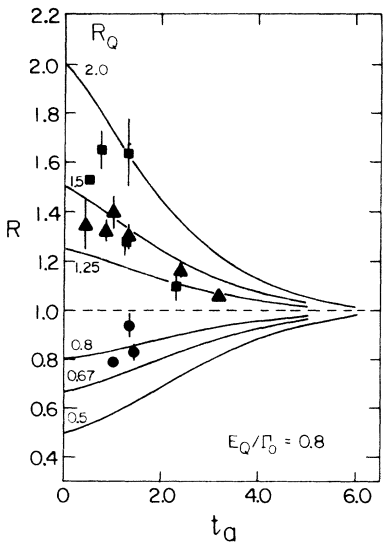

FIG. 7. Variation of the fitted intensity ratio R with absorber thickness for values of the intensity ratio R_Q, defined in the text. The curves show results of fits to theoretical spectra with $E_Q/\Gamma_0 = 0.8$. Data are from runs at or near room temperature on stacks of tin metal foil absorbers with thicknesses 5 μm (circles), 24 μm (triangles), and 130 μm (squares). The data indicate large amounts of texture in each type of polycrystalline foil.

$f_a = 0.040$; if f_a were 0.05, as has also been reported,[22] the data would have shown E_Q increasing with absorber thickness in Fig. 5 together with the inconsistent value $E_Q \sim 0$ in Fig. 6. Results similar to those shown for source B were obtained with the other two sources.

A significant amount of polycrystalline texture was incidentally found in the absorber foils used in the experiment. Figure 7 shows the dependence of the intensity ratio R on t_a for selected values of R_Q and for $E_Q/\Gamma_0 = 0.8$. The data from measurements at or near room temperature on stacks of either 5-, 24-, or 130-μm foils indicate large but different amounts of absorber texture, and yield R_Q equal to 0.8, 1.4, and 1.7, respectively. Such values differ significantly from those which would be caused by vibrational anisotropy alone. At room temperature[23] $\langle x_{\parallel}^2 \rangle / \langle x_{\perp}^2 \rangle = 1.14$, for which it can be shown from Eq. (10) that in the absence of polycrystalline texture R_Q would be equal to 0.95, much closer to unity than the experimental values.

Measurements were carried out for absorbers at temperatures from 4 to 450 K using all three sources. Absorber thicknesses were chosen so that t_a was in the range $t \leq 360$ K, and from the relative areas of spectra found in the present experiments for $T > 360$ K. E_Q was deduced in each case from the splitting Δ using Fig. 5.

V. RESULTS

The values $E_Q/\Gamma_0 = 0.776(44)$, $0.828(23)$, and $0.829(17)$ were determined from the three series of measurements on tin metal at 296 K with sources A, B, and C, respectively, as described in Sec. V. The errors quoted reflect the spread of individual values of E_Q obtained in each series of measurements. The weighted average $E_Q/\Gamma_0 = 0.824(13)$ was adopted.

In arriving at this result the effects of absorber thickness and texture have been accounted for, and source thickness and granularity contributions to the linewidth have been considered. However, the yet unexplained residual line broadening $0.09\Gamma_0$ (Sec. III) may produce a small systematic error in the resulting values of E_Q. This error may be approximately estimated.

It was assumed that this broadening was associated with a corresponding increase in the fitted splitting Δ, the two being proportionately equal to the effects produced by absorber thickness. From Figs. 5 and 6, or from Fig. 4, it may be seen that $(d\Delta/dt_a)/(d\Gamma/dt_a) \approx 0.35$ for $E_Q/\Gamma_0 \approx 0.8$, whence the linewidth broadening $0.09\Gamma_0$ indicates the increase of the splitting $0.35 \times 0.09\Gamma_0 = 0.032\Gamma_0$. This correction factor was subtracted from all values of E_Q found initially using Fig. 5. The uncertainty in this correction factor is assumed to be of the same order as the correction, namely, $0.03\Gamma_0$.

The corrected room-temperature value $E_Q/\Gamma_0 = -0.792(33)$ or $-0.253(10)$ mm sec^{-1} yields an interaction frequency $e^2Qq/h = -9.73(40)$ MHz. The sign of e^2Qq was determined to be negative in Ref. 24.

This value is in good agreement with $e^2Qq/h = -9.07(32)$ MHz obtained by $e^- - \gamma$ TDPAC.[25]

It was suggested in Ref. 25 that the TDPAC method is superior to the Mössbauer method for determining the quadrupole splitting when the splitting is less than the natural linewidth. Although the TDPAC measurement is more precise than the earlier Mössbauer measurements, the precision obtained in the present experiment is comparable. It may be noted that both methods have complementary difficulties caused by the short mean life in the Mössbauer level. The time dependence of the TDPAC perturbation function for the spin-$\frac{3}{2}$ level may be written $\cos[(E_Q/\Gamma_0)(t/\tau)]$. Supposing that at least one complete precision period must be observed in order to extract the quadrupole splitting E_Q reliably, a coincidence-measurement time greater than about $2\pi\tau/(E_Q/\Gamma_0)$ is required, or eight mean lives. In fact, the TDPAC spectrum[25] was measured over eight mean lives, requiring a very long run time. Hence, the case required in analyzing small Mössbauer splittings is balanced by the difficult task of accumulating the corresponding TDPAC spectrum over many lifetimes. An advantage of the Mössbauer method is derived from the "singles" mode of data acquisition, allowing for rapid accumulation of spectra with sources of much higher activity than can be employed in the coincidence mode.

The temperature dependence of e^2Qq/h is shown in Fig. 8 with the average room-temperature measurement indicated by the square, and measurements at other temperatures indicated by circles; the bars show the statistical errors. The TDPAC measurement[25] is also indicated in Fig. 8 (triangle).

Empirically, the temperature dependence of the quadrupole interaction in noncubic metals has been found[26] to be well described by a $T^{3/2}$ law

$$e^2Qq(T)/e^2Qq(0) = 1 - BT^{3/2} \quad . \tag{15}$$

The curve in Fig. 8 shows the result of a fit of the data to that relation, for which $e^2Qq(0)/h = -11.05(5)$ MHz, and $B = 2.25(11) \times 10^{-5}\ \mathrm{K}^{-3/2}$. Values of $e^2Qq(0)/h$ and B from this experiment and from measurements on other probes are listed in Table II. The coefficients B describing the temperature dependence are probe dependent,[27] although this dependence has not yet been explained. However, excepting the large value of B for ^{115}Te, they are roughly consistent with the total EFG decreasing by about 25% over the range 0–500 K.

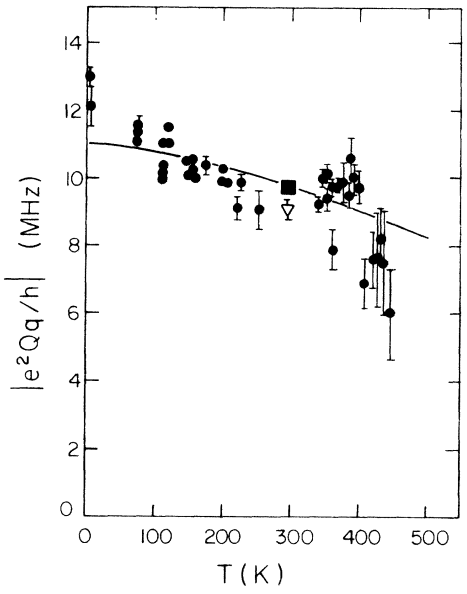

FIG. 8. Temperature dependence of the quadrupole interaction of the Mössbauer level of ^{119}Sn in tin metal. The circles and the square show the results of the present Mössbauer measurements. The square shows the average of all room-temperature measurements. The solid line is the resulting fit of the data to a $T^{3/2}$ temperature dependence. The triangle was obtained from a TDPAC measurement on the same nuclear level (Ref. 25).

TABLE II. $e^2Qq(T)/h$ for different probes in tin metal and the value of the coefficient B obtained from the fit to a $T^{3/2}$ temperature dependence.

Probe	Level (keV)	$\lvert e^2Qq(0)\rvert/h$ (MHz)	B (10^{-5} K$^{-3/2}$)	Reference
^{67}Ge	734	49.0	+1.98(47)	a
^{111}Cd	247	43.4(1)	+3.03(4)	b
^{117}In	659	55.6(5)	+2.01(13)	c
^{119}Sn	23.8	11.05(5)	+2.25(11)	d
^{115}Te	279	6.83(9)	+6.36(18)	e

[a]W. Bartsch, B. Lamp, W. Leitz, H.-E. Mahnke, W. Semmler, and Th. Wichert, International Conference on Applications of the Mössbauer Effect, Leuven, 1975 (unpublished). The normalized frequencies were obtained from Fig. 1 and the four data for $T > 190$ K were fitted with Eq. (15), using the frequency at 448 K from Table I in W. Bartsch, W. Leitz, H.-E. Mahnke, R. Sielemann, and Th. Wichert, International Conference on Hyperfine Interactions Studied in Unclear Reactions and Decay, Uppsala, 1974 (unpublished), p. 216.

[b]Reference 26.

[c]S. H. Devare and H. G. Devare, International Conference on Applications of the Mössbauer Effect, Leuven, 1975 (unpublished). The data from Table I were fitted with Eq. (15).

[d]This experiment.

[e]Quoted in Ref. 26.

VI. DISCUSSION

The total electric-field gradient eq was evaluated at 4, 300, and 500 K from the fit of the experimental data to a $T^{3/2}$ temperature dependence.[7] The EFG is now compared to calculations of the lattice contribution $eq_{\text{latt}}(1-\gamma_\infty)$ and of the conduction-electron contribution eq_{ce}.

The gradient eq_{latt}, due to a lattice of point ions, was calculated by the method of de Wette[4] as a function of the lattice parameters of tin. This calculation is described in Appendix B. The shielding factor[2] used was $\gamma_\infty = -22.34$.

The conduction-electron contribution eq_{ce} was calculated from the space density of all occupied electron states within the Fermi volume using the procedure described in Ref. 1. The theoretical wave functions were obtained by the augmented-plane-wave (APW) method and the integrals were carried out over the volume of the muffin-tin sphere surrounding the nucleus. Details of the APW calculation and complete results will be given in a subsequent publication. The effects of lattice vibrations on the conduction-electron wave functions were explicitly taken into account by insertion of Debye-Waller factors into the matrix elements of the calculation, following the method used by Kasowski for calculating the temperature dependence of the Knight shift in cadmium.[28] For this purpose the atomic mean-squared displacements appear in the Debye-Waller factors were obtained from the recoilless fraction measurements of Ref. 19 and this work. In Table III are listed the calculated values of $eq_{\text{latt}}(1-\gamma_\infty)$, eq_{ce}, and their sum $(eq)_{\text{calc}}$, the theoretical value for the total EFG, and of the ratio $(eq)_{\text{calc}}/eq$ of the theoretical-to-experimental values of the total EFG. Finally, empirical values of the conduction electron contribution defined by $eq_{\text{ce}} = eq - eq_{\text{latt}}(1-\gamma_\infty)$ are also given.

As is commonly observed in most noncubic metals, eq_{ce} and $eq_{\text{latt}}(1-\gamma_\infty)$ have opposite signs. However, in tin, the relative magnitude of $eq_{\text{latt}}(1-\gamma_\infty)$ is unusually small. Empirically, the ratio $eq_{\text{ce}}/eq_{\text{latt}}(1-\gamma_\infty)$ has been found to be equal to approximately -3 in most cases studied.[5] For tin this ratio is much larger and in addition is strongly temperature dependent. At room temperature the ratio obtained in Sn from this experiment is -18, and decreases from -34 at 4 K to -12 at 500 K. Such a large decrease is unusual in the iron cubic metals which have been studied,[29] and is due primarily to the strong increase of eq_{latt} with temperature.

The magnitude of $(eq)_{\text{calc}}$ is seen from Table III to be larger than eq by a factor of about 2.5. This discrepancy is due in part to the various approximations in the calculation of $(eq_{\text{ce}})_{\text{calc}}$, which will be discussed in the paper describing details of the APW calculation and in part to the uncertainty in the value of the quadrupole moment Q. The temperature dependence, however, may be expected to be much more accurate since it is only determined by relative differences. $(eq)_{\text{calc}}$ was fitted to the $T^{3/2}$ dependence to obtain $B = 3.47 \times 10^{-5}\ \text{K}^{-3/2}$, corresponding to a decrease of 40% between 4 and 500 K. The experimental EFG at ^{119}Sn decreased by 25% over the same range (Table II).

The large ratio of $eq_{\text{ce}}/eq_{\text{latt}}(1-\gamma_\infty)$ for tin may be interpreted in light of the unusual axial ratio c/a of the tin lattice. Most noncubic metals and alloys have the hexagonal-close-packed (hcp) structure with axial ratios close to the ideal hcp ratio 1.633. For these metals eq_{latt} varies linearly with the difference $(c/a - 1.6345)$,[4,30] and empirical values of eq_{ce} for a given probe are roughly proportional to eq_{latt} or to $(c/a - 1.633)$.[5,31,32] This proportionality of eq_{latt} with the deviation of c/a from the ideal hcp axial ratio is also indicated from results of a band-structure calculation of the pressure dependence of eq_{ce} in cadmium,[33] although the volume and axial ratio variations were not separately calculated in that study. Thus eq_{latt} and eq_{ce} both appear to be proportional to $(c/a - 1.633)$ in good approximation in the hcp metals.

For the face-centered-tetragonal (fct) structure of indium and indium-rich alloys, both eq_{latt} and eq_{ce} must vanish for $c/a = 1$, owing to cubic symmetry about the nucleus, and for axial ratios close to one, both gradient contributions may be expected to vary

TABLE III. Measured and calculated lattice and conduction-electron electric-field gradients in tin metal. The quadrupole moment of the excited state in ^{119}Sn was taken from Ref. 7, $Q = -0.06(2)$ b. The semiexperimental eq_{ce} is obtained by subtracting the calculated lattice contribution from the total measured electric-field gradient $eq_{\text{ce}} = eq - eq_{\text{latt}}^{\text{calc}}(1-\gamma_\infty)$.

T (K)	e^2Qq/h (MHz)	eq	$eq_{\text{latt}}^{\text{calc}}(1-\gamma_\infty)$	$(eq_{\text{ce}})_{\text{calc}}$	$(eq)_{\text{calc}}$	eq_{ce}	$(eq)_{\text{calc}}/eq$
		←		(10^{17} V cm^{-2})		→	
4	−11.05	+7.62	−0.23	+21.96	+21.73	+7.85	2.85
300	−9.76	+6.73	−0.39	+17.38	+16.99	+7.12	2.52
500	−8.27	+5.70	−0.54	+14.34	+13.80	+6.24	2.42

linearly with the difference $c/a-1$. Such behavior has indeed been found in calculations of eq_{latt},[4] and NMR measurements on indium-rich alloys[34] show the same linear dependence of eq_{ce} on the axial ratio over a range of c/a from 1.05 to 1.10.

Thus in the hcp and fct metals, both eq_{latt} and eq_{ce} are proportional to the difference between c/a and the corresponding ideal axial ratio lying close by. Such behavior might also be anticipated for the semimetals As, Sb, and Bi with the arsenic structure which exhibit small lattice distortions form cubic symmetry.

The tin metal structure, by contrast, results from a large distortion away from cubic symmetry. The observed axial ratio $c/a \approx 0.545$ is much smaller than the ratio $c/a = 1.414$ at which the diamond structure is obtained, so that one cannot reasonably expect either eq_{latt} or eq_{ce} to vary linearly with the difference $c/a-1.414$. In Appendix B it is shown that for tin metal c/a is quite close to the value 0.540 068 for which eq_{latt} is accidentally equal to zero. eq_{latt} varies as $c/a-0.540\,068$ over the experimental range of c/a, from 0.5433 to 0.5479. In additional APW calculations of eq_{ce} cited above, it was found that for a rigid lattice and at constant volume, eq_{ce} changes by less than 0.5% over that range of c/a, while eq_{latt} and eq_{ce} vary differently with changing axial ratio, unlike the situation found in the hcp and fct metals.

The degree of independence of eq_{ce} on eq_{latt} in tin metal might be tested experimentally by quadrupole-interaction measurements on tin-rich alloys similar to the NMR measurements made on indium-rich alloys.[34] For the tin alloys, the axial ratio can be varied[35] at room temperature from 0.5447 to 0.5462, over which range eq_{latt} increases by 28%. Contrary to the conclusion reached here that eq_{ce} and eq_{latt} are independent of each other, if they were linearly correlated as in the hcp and fct metals, eq would similarly increase by 28%. Such a variation could be readily measured.

ACKNOWLEDGMENT

This work was supported in part by the NSF.

APPENDIX A: GRANULAR MÖSSBAUER SOURCES

Mössbauer sources, especially those involving isomeric transitions such as $^{119}Sn^{m}$ and $^{83}Kr^{m}$, often contain ground-state nuclei of the Mössbauer nuclide. The emission profile is then broadened by resonant self-absorption of the emitted γ rays. For a single line source which is uniform both in chemical composition and in thickness, the recoilless contribution to the emission profile was given by Eq. (13).

Additional line broadening appears when the thickness of the emitting material is variable across the area of the source. The variation of the source thickness may be described by a probability $D(t)$ that an area element of the source has a resonant absorption thickness parameter between t and $t+dt$, where the parameter t is proportional to the variable physical thickness. $D(t)$ must satisfy the relations

$$\int D(t)\,dt = 1$$

and

$$\int tD(t)\,dt = t_s \ .$$

It is assumed below that m, the ratio of the nonresonant-to-resonant absorption thicknesses, is independent of local source thickness. This assumption is adequate for the powder $BaSnO_3$ sources used in this experiment, since lucite, which has a relatively small mass absorption at 24 keV, filled the inactive volumes of the sources.

The broadened emission profile $\overline{W}_e(x;t_s,m)$ is equal to the average of the emission profiles for thickness t weighted by the activity for each thickness, which is itself proportional to t,

$$\overline{W}_e(x;t_s,m) = \int_0^\infty tD(t)\,W_e(x;t,m)\,dt \times \left[\int_0^\infty tD(t)\,dt\right]^{-1} = \frac{1}{t_s}\int_0^\infty tD(t)\,W_e(x;t,m)\,dt \ . \quad \text{(A1)}$$

Substituting $W_e(x;t,m)$ from Eq. (13), we have

$$\overline{W}_e(x;t_s,m) = \frac{f_s}{\pi t_s}\frac{l(x)}{m+l(x)} \times \int_0^\infty D(t)\{1-\exp\{-t[m+l(x)]\}\}\,dt \quad \text{(A2)}$$

and Γ is obtained by solving $\overline{W}_e(x;t_s,m) = \frac{1}{2}\overline{W}_e(0;t_s,m)$.

Three simple models for the distribution $d(t)$ were investigated.

A. Monolayer grain model

If the source consists of grains of thickness $t_g = rt_s$ distributed in a monolayer across the source, then for $r > 1$,

$$D(t) = [(r-1)/r]\delta(t) + (1/r)\delta(t-rt_s) \quad \text{(A3)}$$

and δ is the delta function. Then we have

$$\overline{W}_e(x;t_s,m) = \frac{f_s}{\pi t_s}\frac{l(x)}{m+l(x)}\frac{1}{r} \times (1-\exp\{-rt_s[m+l(x)]\}) \ . \quad \text{(A4)}$$

For this model, $\overline{W}_e(x;t_S,m) = W_e(x;rt_S,m)$; the profile is the same as for a uniform source but with an effective thickness $t_S^{\text{eff}} = t_g = rt_S$. For $r < 1$ the source thickness may be assumed to be approximately uniform so that $t_S^{\text{eff}} = t_S$. This variation of t_S^{eff}/t_S with r is shown by curve a in Fig. 9.

B. Poisson-distribution model

Suppose the source consists of grains of thickness $t_g = rt_S$ which are randomly distributed through the (semi-infinite) source volume. The probability of finding n grains in a row is then given by the Poisson distribution $P_n = e^{-\bar{n}}\bar{n}^n/n!$, in which the mean number of grains $\bar{n} = 1/r$. Then

$$D(t) = \sum_{n=0}^{\infty} P_n \delta(t - nrt_S) \quad , \tag{A5}$$

and it is readily found that

$$\overline{W}_e(x;t_S,m) = \frac{f_S}{\pi t_S}\frac{I(x)}{m + I(x)} \times \left[1 - \exp\left(-\frac{1 - \exp\{-rt_S[m + I(x)]\}}{\quad}\right)\right] \tag{A6}$$

Γ_S may then be found as described above. In the limit $r \to 0$, Eq. (A6) is equal to Eq. (13), so that $t_S^{\text{eff}} = t_S$. For large r, $D(t)$ approaches the monolayer distribution and $t_S^{\text{eff}} \to rt_S$ since the probability of finding more than one grain in a row becomes vanishingly small. There is no expression for t_S^{eff} valid for arbitrary t_S, m, and r that yields the exact emission profile in the functional form $W_e(x;t_S^{\text{eff}},m)$ of Eq. (13), but upper and lower limits on t_S^{eff} exist as a function of r. The upper limit is given by the average of t, weighted by the activity ($\sim t$),

$$\frac{\langle t^2\rangle}{\langle t\rangle} = \sum_{n=0}^{\infty} P_n (nrt_S)^2 \left[\sum_{n=0}^{\infty} P_n (nrt_S)\right]^{-1} = (1 + r)t_S \tag{A7}$$

(curve b, Fig. 9). t_S^{eff} must be smaller than $(1 + r)t_S$ since self-absorption decreases relatively the flux of the emergent γ rays from the thicker surface elements. The lower limit is given by the effective thickness for a monolayer, since the emission from elements with more than one grain in a row will broaden the emission profile. The region of possible t_S^{eff} for the Poisson-distribution model is indicated by the shading on Fig. 9. Empirically, t_S^{eff} was found to be described approximately by $(r + e^{-r/2})t_S$ (curve c, Fig. 9).

C. Thickness distribution

As a final example, for the continuous thickness distribution,

$$D(t) = \begin{cases} \frac{1}{2}T & \text{for } t_S - T < t < t_S + T \\ 0 & \text{otherwise,} \end{cases} \tag{A8}$$

in which $T < t_S$, it is easily shown that

$$\overline{W}_e(x;t_S,m) = \frac{f_S}{\pi t_S}\frac{I(x)}{m + I(x)} \times \left[1 - \frac{\sinh\{T[m + I(x)]\}}{T[m + I(x)]} \times \exp\{-t_S[m + I(x)]\}\right] . \tag{A9}$$

The thickness distribution $D(t)$ of the two stannate

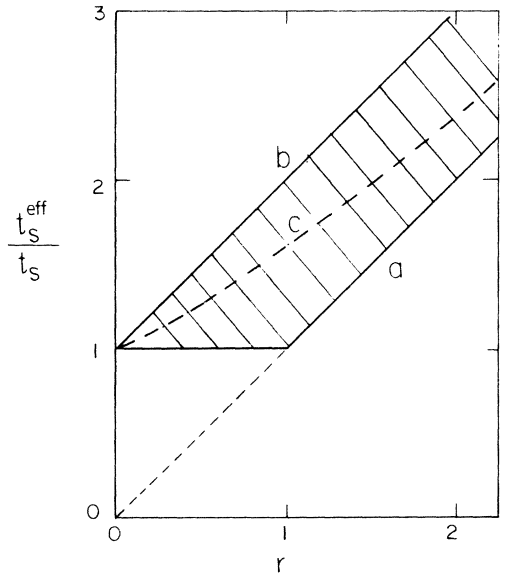

FIG. 9. Dependence of the effective resonant absorber thickness parameter t_S^{eff} for a granular Mössbauer source on the ratio r of the thickness of a grain to the average source thickness.

TABLE IV. Parameters describing the granularity of the $BaSnO_3$ sources. r is equal to the ratio of t_g, the grain thickness, to t_S, the source thickness parameter.

Source	A	B
t_S	1.95	0.50
t_S^{eff} (Monolayer model)	2.40	0.73
r (Monolayer model)	1.23	1.46
r (Poisson-distribution model)	0.76	0.81
r (Observed visually)	0.1–2.5	0.1–2.5

TABLE V. Dependence of the lattice EFG in tin metal on the axial ratio.

c/a	a^3q_{latt}/Z	c/a	a^3q_{latt}/Z
0.3	122.234 77	0.7	−8.062 72
0.4	33.297 13	0.8	−8.462 60
0.5	5.263 92	0.9	−7.547 55
0.54	0.007 26	1.0	−6.072 69
0.540 068	0.000 00	1.2	−2.835 55
0.542	−0.203 89	1.4	−0.157 95
0.543	−0.307 87	1.414 214	0.000 00
0.544	−0.410 81	1.6	1.662 66
0.545	−0.512 71	1.8	2.705 03
0.546	−0.613 57	2.0	3.152 03
0.547	0.713 40	2.5	2.775 32
0.548	0.812 23	3.0	1.593 74
0.549	0.919 06	3.657 30	0.000 00
0.6	−4.765 04	4.0	−0.716 71

sources used in the experiment could not be measured precisely, although visual observations showed grains varying in size from 0.1 to 2.5 times the average thicknesses. However, the additional source line broadenings can be shown to be compatible with these grain sizes.

For source A, the emission linewidth Γ_s due to source absorption and granularity alone was $1.54\Gamma_0$. The effective thickness in the monolayer model is equal to that value of t_s at which $\Gamma_s = 1.54\Gamma_0$, for $m = 0.39$, Eq. (13) yielded $t_s^{\text{eff}} = 2.40$. This value may also be obtained graphically from Fig. 2. The grain size estimate $r = t_s^{\text{eff}}/t_s = 1.23$ is then obtained. Within the Poisson-distribution model, the equation

$$\overline{W}_c(1.54; t_s, m) = \tfrac{1}{2}\,\overline{W}_c(0; t_s, m)$$

was solved numerically, yielding the value $r = 0.76$. Both estimates for the grain size are consistent with the mean of the observed grain thicknesses. Similar analysis for source B leads to the same conclusion. The grain-size estimates for each source, as deduced from the monolayer and Poisson-distribution models and from observation, are given in Table IV.

APPENDIX B: LATTICE EFG IN TIN METAL

The method of de Wette[4] was used to calculate the gradient eq_{latt} of a lattice of point ions in tin metal. For this purpose the lattice, with space group D_{4h}^{19}, may be considered to consist of four interpenetrating simple tetragonal sublattices with basis vectors (0,0,0), $(\frac{1}{2},\frac{1}{2},\frac{1}{2},)$, $(\frac{1}{2},0,\frac{1}{4})$, and $(0,\frac{1}{2},\frac{3}{4})$ in units of the lattice constants (a,a,c). The gradient is given in the notation of Ref. 4 by

$$a^3q/Z = 32\pi/3\alpha + a^3(S^{\text{tetr}}_{0,0,0} + S^{\text{tetr}}_{1/2,1/2,1/2,} + S^{\text{tetr}}_{1/2,0,1/4} + S^{\text{tetr}}_{0,1/2,1/4}), \tag{B1}$$

in which $\alpha = c/a$ is the axial ratio and Z is the ionic charge. The factor $32\pi/3\alpha$ is the contribution from a uniform background of conduction electrons over a slab-shaped region and arises from the calculation. $S^{\text{tetr}}_{l,l',l''}$ are lattice sums over the four tetragonal sublattices. From Eqs. (8) and (14) in Ref. 4, one finds

TABLE VI. Lattice EFG in tin metal. The lattice constants are obtained from Refs. a–c. The values at 500 K were extrapolated from data in Ref. c. a^3q_{latt}/Z was calculated using Eq. (B2). The ion charge $Z = 4$ was used to evaluate eq_{latt}.

		4 K	300 K	500 K
c	(a_0)	5.965 8	6.013 4	6.063 3
a	(a_0)	10.983 0	11.020 6	11.066 7
c/a		0.543 28	0.545 65	0.547 89
a^3q_{latt}/Z		−0.335 66	−0.577 26	−0.800 37
eq_{latt}	$(10^{17}\text{V cm}^{-2})$	−0.009 85	0.016 77	−0.022 96

[a]J. A. Rayne and B. S. Chandrasekhar, Phys. Rev. 120, (1960) 1658.
[b]H. W. King and T. D. Massalski, J. Inst. Met. 90, 486 (1962).
[c]V. T. Desphande and D. B. Sirdeshmukh, Acta Crystallogr. 15, 294 (1962).

$$\frac{a^3q}{Z}=\frac{32\pi}{3\alpha}-9.033\,621\,7+4\pi^2\sum_{m,n}{}'\frac{h\{\exp(-\pi h\alpha)+(-1)^{m+n}+[(-1)^m+(-1)^n]\cosh(\frac{1}{2}\pi h\alpha)\}}{\sinh(\pi h\alpha)}\,, \tag{B2}$$

where $h=(m^2+n^2)^{1/2}$ and the summations run over all integers m and n except $m=n=0$. The summations converged to within eight decimal places for sums m,n over the ranges ± 50. The dependence of a^3q_{latt}/Z on the axial ratio, calculated using Eq. (B2), is tabulated in Table V.

The gradient is zero for three values of the axial ratio. At $c/a=\sqrt{2}$, the tin metal structure is isomorphous with the cubic diamond lattice and all EFG contributions vanish. Zeros of eq_{latt} unrelated to crystal symmetry also occur at $c/a=0.540\,068$ and $3.657\,30$. From the measured lattice parameters and the deduced values of eq_{latt} (Table VI) the axial ratio is seen to fall quite close to the zero at 0.540 068. From 4 to 500 K the lattice gradient increases by the factor 2.33 while the axial ratio changes by only 0.8%. The dramatic increase of eq_{latt} with temperature is large when compared to the variations calculated in other metals.[36]

As a final remark, it may be noted that eq_{latt} is not explicitly affected by lattice vibrations on a time average as long as the mean-square displacements of atoms are isotropic. To a very good approximation, eq_{latt} only depends on the volume and axial ratio of the unit cell.

[1]T. P. Das, Phys. Scr. 11, 121 (1975).

[2]F. D. Feiock and W. R. Johnson, Phys. Rev. 187, 39 (1969).

[3]R. M. Sternheimer, Phys. Rev. 164, 10 (1967).

[4]F. W. de Wette, Phys. Rev. 123, 103 (1961).

[5]R. S. Raghavan, E. N. Kaufmann, and P. Raghavan, Phys. Rev. Lett. 34, 1280 (1975); R. S. Raghavan, Hyperfine Interactions 2, 29 (1976).

[6]G. S. Collins, Ph.D. thesis (Rutgers University, 1976) (unpublished).

[7]S. L. Ruby, G. M. Kalvius, G. B. Beard, and R. E. Snyder, Phys. Rev. 159, 239 (1967).

[8]The quadrupole splittings from the earlier Mössbauer measurements and references may be found in Ref. 25. See also W. Singer, Hyperfine Interactions 2, 254 (1976).

[9]The sources were purchased from New England Nuclear Corp., North Billerica, Mass. 01862.

[10]R. K. Puri, Nucl. Instrum. Methods 117, 381 (1974).

[11]Purchased from Ventron Inorganics Division, Alfa Corp., Beverly, Mass. 01915.

[12]S. Margulies and J. R. Ehrman, Nucl. Instrum. Methods 12, 131 (1961); S. Margulies, P. Debrunner, and H. Frauenfelder, *ibid.* 21, 217 (1963).

[13]*Mössbauer Effect Data Index: 1973,* edited by J. G. Stevens and V. E. Stevens (Plenum, New York, 1975).

[14]The quoted lifetime is the average of measurements from N. Benczer-Koller and T. Fink, Nucl. Phys. A 161, 123 (1971), H. Drost, W. Weiss, and G. Weyer, Z. Naturforsch. A 26, 1092 (1971); and M. C. Abreu and F. B. Gil, J. Phys. G 2, 51 (1976).

[15]G. A. Bykov and Pham Zuy Hien, Sov. Phys.-JETP 16, 646 (1963).

[16]See, for example, V. I. Goldanskii and E. F. Makarov, in *Chemical Applications of Mössbauer Spectroscopy,* edited by V. I. Goldanskii and R. H. Herber (Academic, New York, 1968), p. 1.

[17]U. Gonser and H.-D. Pfannes, J. Phys. (Paris) 35, C 6-113 (1974).

[18]See, for example, E. Gerdau, W. Rath, and H. Winkler, Z. Phys. 257, 29 (1972); R. E. Meads, B. M. Place, F. W. D. Woodhams, and R. C. Clark, Nucl. Instrum. Methods 98, 29 (1972); S. A. Wender and N. Hershkowitz, *ibid.* 98, 105, (1972); and G. Hembree and D. C. Price, *ibid.* 108, 99 (1973).

[19]C. Hohenemser, Phys. Rev. 139, 185 (1965).

[20]The f values obtained in Ref. 19 are not significantly affected by the quadrupole splitting, although the splitting was not explicitly considered.

[21]J. D. Bowman, E. Kankeleit, E. N. Kaufmann, and B. Persson, Nucl. Instrum. Methods 50, 13 (1967).

[22]A. Biran., A. Yarom, P. A. Montano, H. Shechter, and U. Shimony, Nucl. Instrum. Methods 98, 41 (1972).

[23]The ratio $f_a(\theta=0°)/f_a(\theta=90°)=0.65$ at 300 K was measured by N. E. Alekseeviskii and A. P. Kir'yanov, JETP Lett. 9, 53 (1969).

[24]N. E. Alekseevskii, Pham. Suy Hien, V. G. Shapiro, and V. S. Shpinel', Sov. Phys.-JETP 16, 559 (1963).

[25]J. C. Soares, K. Krien, A. G. Bibiloni, K. Freitag, and R. Vianden, Phys. Lett. A 45, 465 (1973).

[26]J. Christiansen, P. Heubes, R. Keitel, W. Klinger, W. Loeffler, W. Sander, and W. Witthuhn, Z. Phys. B 24, 177 (1976).

[27]See Table 5 and Fig. 7 in Ref. 26.

[28]R. V. Kasowski and L. M. Falicov, Phys. Ref. Lett. 22, 100 (1969) R. V. Kasowski, Phys. Rev. 187, 891 (1969).

[29]P. Raghavan, E. N. Kaufmann, R. S. Raghavan, E. J. Ansaldo and R. A. Naumann, Phys. Rev. B 13, 2835 (1976).

[30]T. P. Das and M. Pomerantz, Phys. Rev. 123, 2070 (1961).

[31]J. A. Sawicki, Phys. Status Solidi B 53, K 103 (1972).

[32]G. Wortmann and D. L. Williamson, Hyperfine Interactions 1, 167 (1975).

[33]N. C. Mohapatra, C. M. Singal, and T. P. Das, Phys. Rev. Lett. 31, 530 (1973).

[34]F. C. Thatcher and R. R. Hewitt, Phys. Rev. B 1, 454 (1970).

[35]J. A. Lee and G. V. Raynor, Proc. Phys. Soc. B 67, 737 (1954).

[36]See, for example, Table 6 in Ref. 26 for the $eq_{\text{latt}}(T)$ in In, Cd, Zn, and Ti. The values for Sn in that table are in error.